Published online 9 February 2017 *Nucleic Acids Research, 2017, Vol. 45, No. 9* **5501–5511**
doi: 10.1093/nar/gkx109

Characterization of human telomere RNA G-quadruplex structures *in vitro* and in living cells using ^{19}F NMR spectroscopy

Hong-Liang Bao[1], Takumi Ishizuka[1], Takashi Sakamoto[2], Kenzo Fujimoto[2], Tamayo Uechi[3], Naoya Kenmochi[3] and Yan Xu[1,*]

[1]Division of Chemistry, Department of Medical Sciences, Faculty of Medicine, University of Miyazaki, 5200 Kihara, Kiyotake, Miyazaki 889-1692, Japan, [2]School of Materials Science, Japan Advanced Institute of Science and Technology, 1-1 Asahi-dai, Nomi, Ishikawa 923-1292, Japan and [3]Frontier Science Research Center, University of Miyazaki, 5200 Kihara, Kiyotake, Miyazaki 889-1692, Japan

Received December 09, 2016; Revised January 26, 2017; Editorial Decision January 28, 2017; Accepted February 06, 2017

ABSTRACT

Human telomeric RNA has been identified as a key component of the telomere machinery. Recently, the growing evidence suggests that the telomeric RNA forms G-quadruplex structures to play an important role in telomere protection and regulation. In the present studies, we developed a ^{19}F NMR spectroscopy method to investigate the telomeric RNA G-quadruplex structures *in vitro* and in living cells. We demonstrated that the simplicity and sensitivity of ^{19}F NMR approach can be used to directly observe the dimeric and two-subunits stacked G-quadruplexes *in vitro* and in living cells and quantitatively characterize the thermodynamic properties of the G-quadruplexes. By employing the ^{19}F NMR in living cell experiment, we confirmed for the first time that the higher-order G-quadruplex exists in cells. We further demonstrated that telomere RNA G-quadruplexes are converted to the higher-order G-quadruplex under molecular crowding condition, a cell-like environment. We also show that the higher-order G-quadruplex has high thermal stability in crowded solutions. The finding provides new insight into the structural behavior of telomere RNA G-quadruplex in living cells. These results open new avenues for the investigation of G-quadruplex structures *in vitro* and in living cells.

INTRODUCTION

RNA structure influences the functions of nearly all classes of RNAs (1–3), including RNA G-quadruplexes, which are four-stranded RNA structures that have emerged as potential targets for drug design because of their biological importance (4–6). For example, RNA G-quadruplexes were recently reported to cause protein-dependent oncogene translation in cancer and neurodegenerative diseases (7,8). Recently, we and other groups demonstrated that human telomere RNA, a newly found telomeric repeat-containing RNA (9,10), forms G-quadruplex structures (11–14). We also found that telomere RNA G-quadruplex structures play an important role in providing a protective structure for telomere ends (15). Recently, some studies have also suggested that telomere RNA G-quadruplexes may form polymorphic higher-order G-quadruplexes comprising two stacked G-quadruplex subunits (16,17). However, direct evidence for human telomeric RNA higher-order G-quadruplexes existing in cells has not yet been obtained. Therefore, a more effective chemical approach for obtaining structural information on telomere RNA G-quadruplexes in living cells is desired.

In the present study, we employed fluorine-19 (^{19}F) NMR spectroscopy of oligonucleotides with fluorine labels to further investigate the structural basis of telomere RNA G-quadruplexes *in vitro* and in living cells. ^{19}F NMR has been successfully used to investigate important conformations of nucleic acids due to the high sensitivity of the ^{19}F chemical shift to the environment, 100% natural abundance of ^{19}F, absence of any natural background signals in RNA and cells and relative simplicity of ^{19}F NMR spectra (18–32).

Thus, using the simplicity and sensitivity of ^{19}F NMR spectroscopy, we directly observed the two-subunits stacked telomere RNA G-quadruplex in living cells, providing the in cell evidence for the presence of the higher-order G-quadruplex in human RNA at first time. The in-cell result suggested that molecularly crowded environment in cells promotes the higher-order G-quadruplex structure formation even at low RNA concentration. It is known

*To whom correspondence should be addressed. Tel: +81 985 85 0993; Fax: +81 985 85 9823; Email: xuyan@med.miyazaki-u.ac.jp
Present address: Takashi Sakamoto, Faculty of Systems Engineering, Wakayama University, 930 Sakaedani, Wakayama, Japan.

that biomolecules function in a crowded intracellular environment. Molecular crowding could affect the structure, stability and conformational transition of biomolecules (33–35). We further demonstrated that telomere RNA G-quadruplexes are converted to the higher-order G-quadruplex under molecular crowding condition and further shown that the higher-order G-quadruplex has high thermal stability in crowded solutions. These results provide valuable information for understanding the structure and function of human telomere RNA.

MATERIALS AND METHODS

Sample preparation

RNA was incorporated a six-ethyl linker and 3,5 bis(trifluoromethyl)phenyl moiety at the 5′ terminal on a 1.0 μmol scale using an automatic DNA/RNA synthesizer using solid-phase phosphoramidite chemistry. After automated synthesis, the oligomer was detached from the support, deprotected and purified by RP-HPLC using an appropriate linear gradient of 50 mM ammonium formate in H_2O and 50 mM ammonium formate in 1:1 acetonitrile/H_2O. The oligomer was desalted by NAP10 column (GE Healthcare) and identified by a matrix-assisted laser desorption/ionization-time-of flight mass spectrometer (MALDI-TOFMS) on an autoflex III smart beam mass spectrometer (negative mode), Calcd. 4376.58, Found. 4379.88.

CD measurement

Circular dichroism (CD) spectra were measured using a Jasco model J-820 CD spectrophotometer. The spectra were recorded using a 1 cm path length cell. Samples were prepared by heating the oligonucleotides at 95°C for 5 min and gradually cooling to room temperature. Solutions for CD spectra were prepared as 0.3 ml samples at a 10 μM strand concentration in the presence of 50 mM KCl, 10 mM Tris-HCl buffer (pH 7.0).

In vitro ^{19}F-NMR spectroscopy

RNA samples of 0.2–5.0 mM were dissolved in 150 μl of designed solvent which containing 10 mM Tris-HCl buffer (pH 7.0) and 50 mM KCl. ^{19}F NMR spectra were measured at a frequency of 376.05 MHz on a Bruker AVANCE 400 MHz spectrometer and were referenced relative to external CF_3COOH (−75.66 ppm). Experimental parameters were as follows: ^{19}F excitation pulse 15.0 μs, spectral width 89.3 kHz, acquisition time 0.73 s, relaxation delay 1 s, number of scans 64 or 512 or 2048, an exponential window function with lb = 0.3 Hz was used, no zerofilling was used. At temperature-dependent experiment, the sample is kept for 10 min at each temperature.

In-cell ^{19}F-NMR spectroscopy

In-cell NMR sample was prepared by direct microinjection 50 nl aliquot of the stock solution (3 and 5 mM of 12-mer RNA) into the oocyte cell (∼150 and ∼250 μM intracellular concentration). Approximately 150 *Xenopus laevis* oocytes were injected by using an IM-30 Electric Microinjector (NARISHIGE, Tokyo). After injection, the oocytes were transferred to a disposable dish, washed carefully with oocyte stocking buffer (15 mM Tris-HCl (pH7.6), 88 mM NaCl, 1 mM KCl, 0.4 mM $CaCl_2$, 0.3 mM $Ca(NO_3)_2$, 0.8 mM $MgCl_2$ and 2.4 mM $NaHCO_3$). The injected oocytes were transferred to a Shigemi tube (Shigemi 5 mm Symmetrical NMR microtube) and kept in an oocyte stocking buffer containing 10% of D_2O. Sample for measurement in lysate was prepared as follows: after the in-cell NMR measurements, oocytes were mechanically crushed and used for NMR measurement.

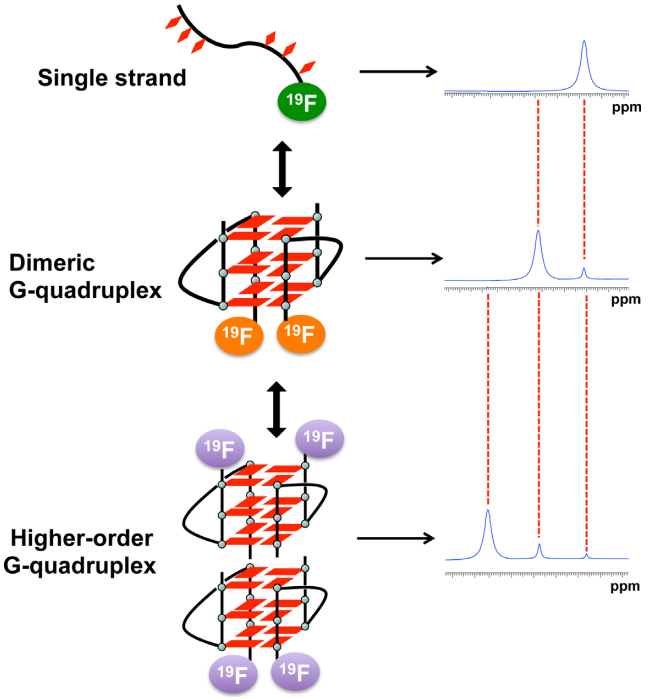

Figure 1. Concept for the detection different RNA structures by a ^{19}F label. Three ^{19}F resonances of different chemical shifts are expected according to single-stranded, dimeric G-quadruplex and two-subunits stacked G-quadruplex.

RESULTS AND DISCUSSION

In vitro ^{19}F NMR analysis of telomere RNA G-quadruplexes

The present study is based on the concept that ^{19}F NMR signals are strongly dependent on the structural environment of the ^{19}F label. Thus, it should be possible to distinguish different RNA structures of the same sequence by the corresponding resonances of the different structures, such as single strands and G-quadruplexes (Figure 1). To achieve this goal, a 3,5-bis(trifluoromethyl)benzene moiety was introduced into 5′ termini of oligonucleotide using phosphoramidite chemistry (Figure 2A and Supplementary Figures S1–S6). The ^{19}F labeling of RNA with six equivalent ^{19}F atoms was expected to afford the high ^{19}F intensity. First, we examined the conformation of the oligonucleotide ORN-1 with the ^{19}F label at 5′ termini by CD spectroscopy. The CD spectrum of ORN-1 in the presence of K^+ at 20°C showed a positive band at 265 nm and a neg-

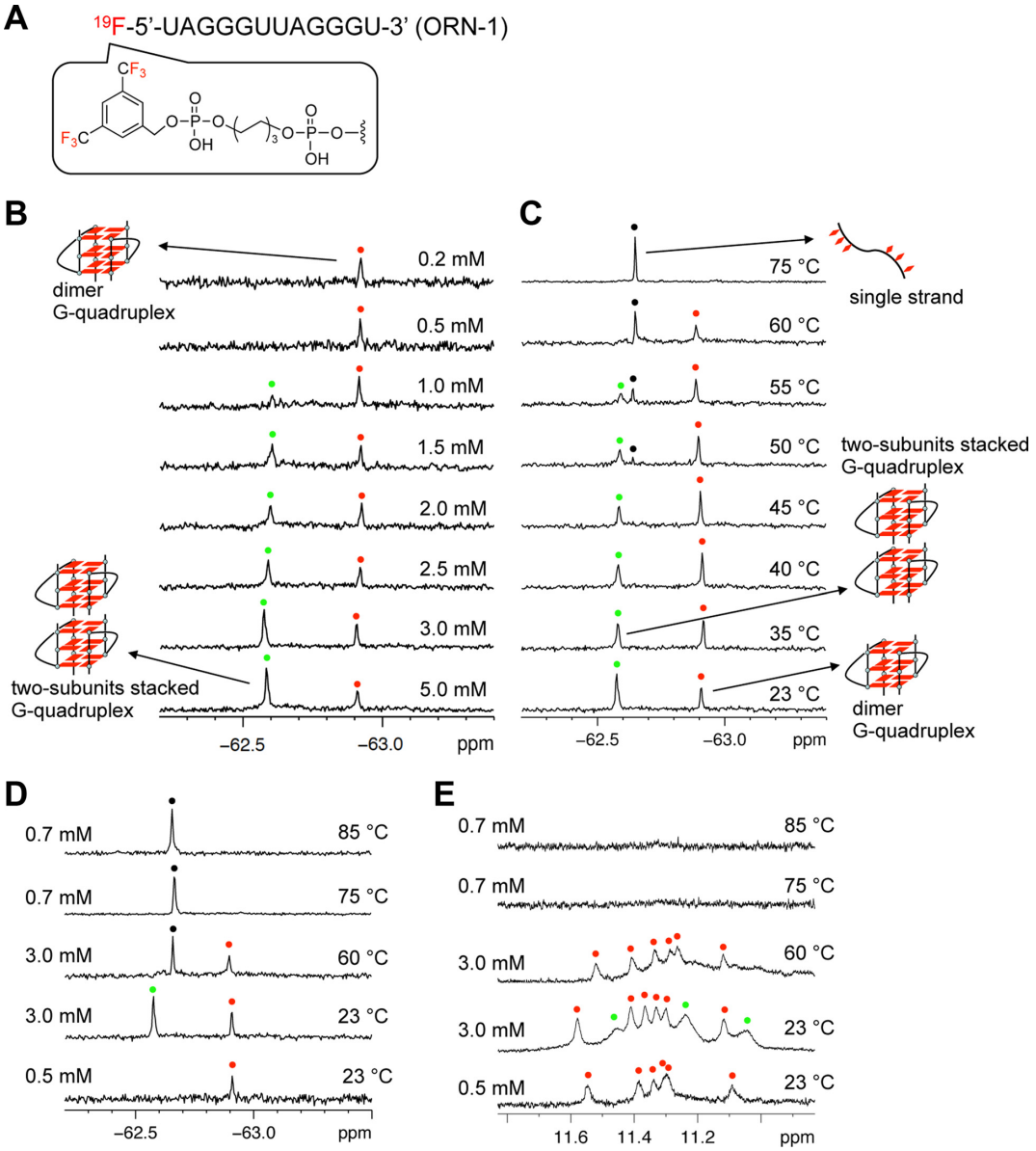

Figure 2. ^{19}F NMR and ^{1}H NMR spectra of ^{19}F labeled RNA. (**A**) Chemical structure of ^{19}F labeled telomere RNA bearing 3,5 bis(trifluoromethyl)phenyl group at the 5′ terminal. (**B**) ^{19}F NMR spectra of ^{19}F labeled telomere RNA at different concentrations. The peaks of the dimeric and two-subunits stacked G-quadruplex are marked with red and green spots, respectively. Concentrations of RNA indicated on the right. (**C**)^{19}F NMR of ^{19}F labeled RNA at different temperatures. Red and green spots indicated dimer and two-subunits stacked G-quadruplex. The peaks of single strand are marked with black spots. Temperatures indicated on the right. Condition: 3 mM RNA in 50 mM KCl and 10 mM Tris-HCl buffer (pH 7.0). The sample is kept for 10 min at each temperature. (**D**) ^{19}F NMR of ^{19}F labeled RNA at different temperatures and concentrations. The peaks of dimer G-quadruplex are red spots. The peak of two-subunits stacked G-quadruplex is green spot. The peaks of single strand are marked with black spots. (**E**) ^{1}H imino proton NMR of ^{19}F labeled RNA corresponding to ^{19}F NMR at different temperatures and concentrations. The peaks characteristic of the dimeric and two-subunits stacked G-quadruplex are marked with red and green spots, respectively.

ative band at 240 nm (Supplementary Figure S7), which are the characteristic CD signatures of a parallel dimeric G-quadruplex structure of RNA consistent with previously reported (11–14), suggesting that the ^{19}F label at 5′ termini does not affect the folding of G-quadruplex. Next, we performed a concentration-dependent experiment to investigate the structural behavior of ORN-1 for the formation of RNA G-quadruplex by ^{19}F NMR (Figure 2B). The ^{19}F NMR spectrum was firstly obtained at 0.2 mM RNA concentration. One signal was observed at −62.91 ppm in the presence of 50 mM KCl, indicating dimer G-quadruplex formation consistent with CD result. As shown in Figure 2B, a new signal appears as the RNA concentration increases (−62.57 ppm). The new signal is clearly observed at an RNA concentration of 1.5 mM, and at 3.0 and 5.0 mM its intensity becomes remarkably greater than that of the initial peak. Each ^{19}F NMR signal arises as a result of the unique fluorine environment; thus, the presence of the two signals confirms the existence of two conformers of the telomere RNA. Accordingly, the two signals were assigned

to the dimeric and two-subunits stacked G-quadruplexes in accord with previous studies that suggested two RNA G-quadruplex subunits are most likely to form a two-subunits stacked G-quadruplex (16,17).

As shown in Figure 3A, profiles of the relative peak areas of the ^{19}F resonance signals versus concentration revealed that a higher RNA concentration promotes the formation of the two-subunits stacked G-quadruplex, suggesting that the of stacking two G-quadruplex subunits is a concentration-dependent manner.

A temperature-dependent experiment was then performed to confirm the assignment of the two signals observed in the ^{19}F NMR spectrum (Figure 2C). As the temperature increased from 23°C to 75°C, the intensity of the signal at −62.57 ppm for the two-subunits stacked G-quadruplex decreased, while that of the signal at −62.91 ppm for the dimeric G-quadruplex increased, indicating the conversion of the two-subunits stacked G-quadruplex to the dimeric G-quadruplex at higher temperatures. Upon heating to 50°C, a new peak at –62.64 ppm corresponding to the unfolded single strand appeared, and at 75°C, only this peak remained with a strong intensity, whereas the peaks of the dimeric G-quadruplex (at −62.91 ppm) and two-subunits stacked G-quadruplex (at −62.57 ppm) completely disappeared. This result indicated that at high temperatures, both the dimer and two-subunits stacked G-quadruplexes unfolded to a single strand.

To further confirm that two subunit G-quadruplexes stack together to form a two-subunits stacked G-quadruplex structure, ^{1}H imino proton NMR analysis was performed. Figure 2E shows the spectrum for a 0.5 mM RNA solution. Six peaks assignable to the dimeric G-quadruplex are observed at 11.0–12.0 ppm that correspond to the peak of the dimeric G-quadruplex in the ^{19}F NMR spectrum (Figure 2D) and are consistent with the results of previous studies (11–14). In the ^{1}H NMR spectrum of a 3 mM RNA solution at 23°C, new signals were observed in addition to major ones (Figure 2E), which was in agreement with the presence of two signals for the dimeric and two-subunits stacked G-quadruplexes in the ^{19}F NMR spectrum (Figure 2D) and suggested that the new signals were due to the two-subunits stacked G-quadruplex structure. Upon heating to 60°C, the new signals disappeared and only the dimeric G-quadruplex peaks were detected in the ^{1}H NMR spectrum (Figure 2E). These observations agreed well with the ^{19}F NMR spectrum at 60°C (Figure 2D), in which signal for the dimeric G-quadruplex appeared. Although signal for the unstructured single strand was observed at ^{19}F NMR at 60°C (Figure 2D), the unstructured single strand does not exhibit any resonance peaks at 11.0–12.0 ppm of the ^{1}H NMR because this region only corresponds to the imino protons of the G-quartet. After complete denaturation (75°C and 85°C), the signals for the dimeric and two-subunits stacked G-quadruplexes were not observed in the ^{1}H NMR spectrum, which is in accordance with the ^{19}F NMR spectrum, in which only the peak for the unstructured single strand was observed.

Encouraged by the ability to use ^{19}F NMR spectroscopy to monitor the conformational transition behavior of the RNA telomere via observation of pronounced changes in the ^{19}F resonances as a function of temperature, the melting process was characterized by plotting the relative peak areas of the ^{19}F resonance signals at various temperatures (Figure 3B). The T_m values for conversion of the two-subunits stacked G-quadruplex to dimeric G-quadruplex and finally to the single strand were estimated to be 52.4°C and 67.8°C, respectively, suggesting stable two-subunits stacked G-quadruplex formation. Importantly, using the corresponding ^{19}F signal curve, a highly precise T_m value was obtained for the two-subunits stacked G-quadruplex, which is not easy to do using other methods, such as CD and ultraviolet spectroscopy, because CD and ultraviolet spectra could not discriminate the higher-order G-quadruplex among different structures.

The presence of resonances for different conformations in the same spectrum at different temperatures allowed quantitative characterization of the thermodynamics of the process (Table 1, and Supplementary Figures S8–S10). The enthalpy change (ΔH) indicates that the stacking interaction of two G-quadruplex subunits is of an enthalpic origin ($\Delta H = -61.8$ kJ/mol). Although conversion from the dimeric G-quadruplex to the single strand involved an unfavorable entropic gain ($\Delta S = -764.9$ J/mol K), large enthalpic contributions to the stability of the G-quadruplex were attributed to the formation of three core G-tetrads ($\Delta H = -260.6$ kJ/mol). Accordingly, the ΔH value for the formation of a single G-tetrad was estimated assuming that the three G-tetrads contribute equally ($\Delta H = -86.9$ kJ/mol $= -260.6 \div 3$). Notably, the ΔH value ($\Delta H = -61.8$ kJ/mol) for the stacking interaction of two G-quadruplex subunits was close to that for the formation of the single G-tetrad, reflecting the significant contribution of the stacking interaction of the two G-quadruplex subunits to the stability of the two-subunits stacked G-quadruplex. These data provide the first evidence that the stacking interactions between two G-quadruplex subunits provide nearly the same energetic contribution as a single G-tetrad.

In-cell ^{19}F NMR analysis of telomere RNA G-quadruplexes

Although *in vitro* ^{19}F NMR spectroscopic methods have made very valuable contributions to our understanding of human telomere RNA structures, *in vivo* observations of RNA G-quadruplex structures are required to gain better insight into the structural basis of their functions inside cells. Indeed, direct evidence for the formation of higher-order G-quadruplexs by human telomere RNA within cells has not yet been obtained.

Recently, developments in NMR technology have made it an effective method for the investigation of biological macromolecules in living cells (in-cell NMR) (36–39). However, the stronger background in the cellular environment often leads to complicated or poor-quality in-cell NMR spectra. For example, ^{1}H imino proton NMR analysis of a telomere DNA G-quadruplex in the cellular environment yields a low-resolution spectrum, thus distinguishing the resonance signals for molecules of interest from the background noise due to the other molecules present in cells remains a challenge (40).

To overcome these limitations, in-cell ^{19}F NMR spectroscopy was employed to investigate the structural features

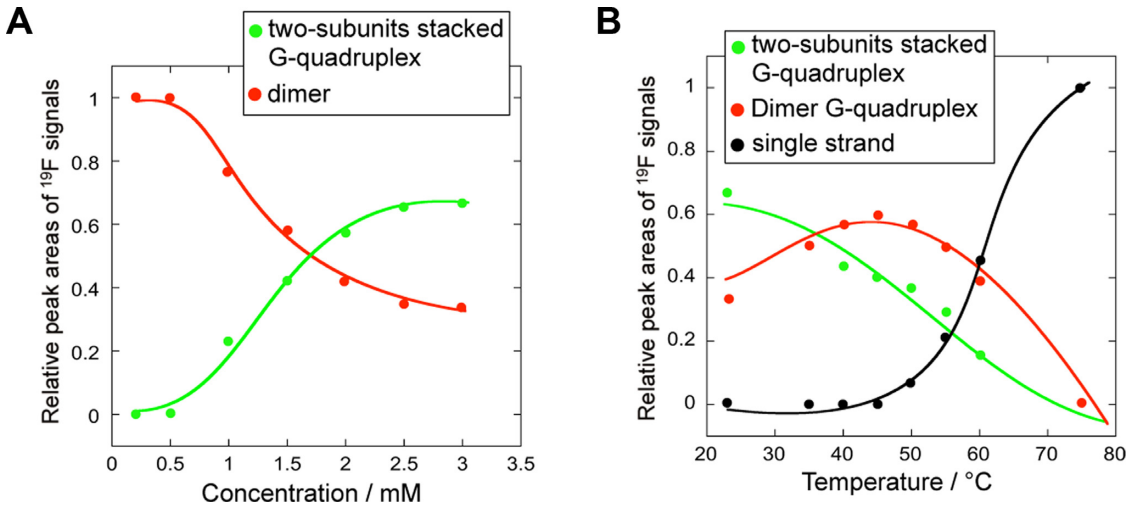

Figure 3. ^{19}F NMR shift versus concentration and temperature profiles. (**A**) Profiles of the relative peak areas of the ^{19}F resonance signals versus concentration. Dimer and two-subunits stacked G-quadruplex conversions followed by ^{19}F NMR spectroscopy. (**B**) Profiles of the relative peak areas of the ^{19}F resonance signals versus temperature. Two-subunits stacked G-quadruplex/dimer G-quadruplex/single strand conversions followed by ^{19}F NMR spectroscopy. To obtain the relative peak signal of each conformation, the total value of the relative peak signal for three conformations was estimated to be 1.0. Plotting the values of relative peak signal against temperature results in two melting curves for the two-subunits stacked Gquadruplex and dimer G-quadruplex.

Table 1. Thermodynamic parameters for RNA conformational transition

RNA conformational transition	$-\Delta H$ (kJ/mol)	$-\Delta S$ (J/mol K)
Two-subunits G-quadruplex → Dimeric G-quadruplex	61.8	186.5
Dimeric G-quadruplex → Single strand	260.6	764.9

[a]The thermodynamic parameters were determined from van't Hoff plots (Supplementary Data). The experimental errors for enthalpy (ΔH) and entropy (ΔS) were ±5 kJ/mol and ±10 J/mol K, respectively.

of human telomere RNA in living cells. Because there is no natural intracellular concentration of fluorine, fluorinated oligonucleotides do not suffer from high background signals. The in-cell NMR study was performed by injecting ^{19}F-labeled telomere RNA into *Xenopus laevis* oocytes and detecting their in-cell conformations using ^{19}F NMR spectroscopy. The strategy used for in-cell ^{19}F NMR spectroscopy is shown in Figure 4A. Nuclei of *Xenopus oocytes* are transferred directly by inserting the glass nuclear transfer pipette into the centre of the animal pole of the oocyte (41,42). The reference *in vitro* spectrum was compared to the in-cell ^{19}F-NMR spectrum, enabling reliable determination of the intracellular telomere RNA conformation. Figure 4B shows a comparison of the *in vitro* and in-cell NMR spectra for the RNA in the pure form (top panel) and upon oocyte injection (bottom panel). Only one signal was observed in the bottom panel NMR spectrum, for which the chemical shift is identical to that observed for the corresponding higher-order G-quadruplex in the *in vitro* ^{19}F NMR spectrum. We further performed an in-cell experiment using low concentration RNA and showed that only one signal, which is same as the chemical shift with high RNA concentration (Supplementary Figure S11), indicating that the two-subunits stacked G-quadruplex structure is still formed at relatively low RNA concentrations. These results demonstrate that the higher-order G-quadruplex structure is present in living cells. The line width of the signal increased in the in-cell spectrum compared to that in the *in vitro* spectrum, partially because of the higher viscosity of the cellular environment (43,44). NMR signals depend on whether the molecule of interest is freely available for tumbling in solution. In general, molecules display small tumbling rates due to their sizes, intermolecular interactions, intramolecular interactions with subsets of residues, and the high viscosity environments of intracellular materials, leading to fast relaxation and broad NMR lines with reduced overall signal intensities. In addition, an inherent sample inhomogeneity due to the in-cell environment is also is the cause of the broad line width of in-cell signal (43,44). A control experiment in oocyte stocking buffer at 0.5 mM RNA concentration was performed to confirm that the formation of high order G-quadruplex does not result from the surrounding oocyte stocking buffer of in-cell experiment. As shown in Supplementary Figure S12, the chemical shift in oocyte stocking buffer is same with dimeric G-quadruplex, indicating that the NMR signal of higher-order G-quadruplex results from inside the cells rather than the surrounding oocyte stocking buffer.

For the further investigation of the influence of molecular crowding, cellular lysates represent a good molecular crowding since they provide a native-like condition. We crushed the oocytes containing the injected RNA and recorded ^{19}F NMR spectrum. Notably, the NMR spectral pattern for the lysate of the telomere RNA is similar to those observed for both the corresponding *in vitro* and in-cell

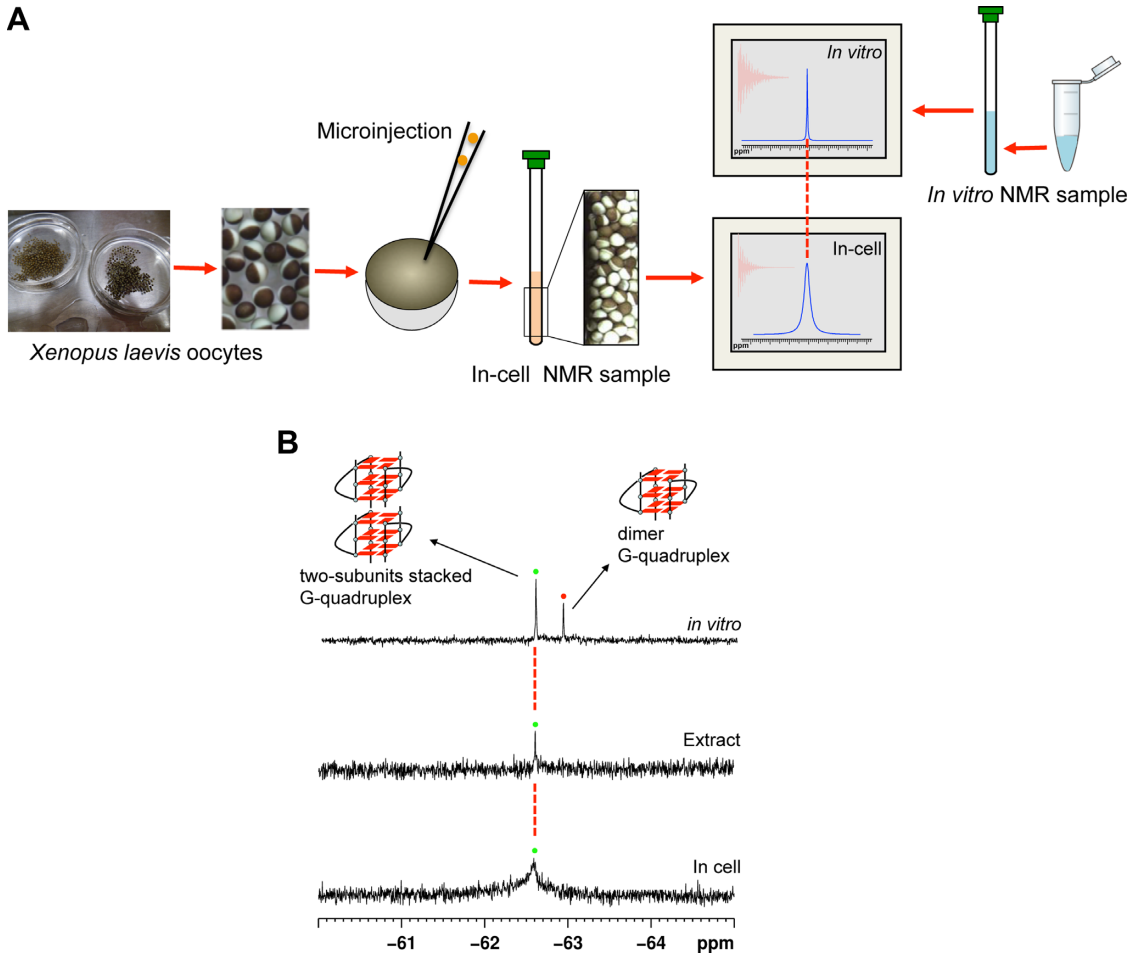

Figure 4. In-cell ^{19}F NMR of telomere RNA G-quadruplex. (**A**) Schematic overview of in-cell ^{19}F NMR experiments. *Xenopus laevis* oocytes are sorted and collected for microinjections. For in-cell ^{19}F NMR applications in *Xenopus* oocytes, telomere RNA sample was injected into the oocyte cells. Comparison with the position of reference *in vitro* spectrum provides a reliable determination of intracellular telomere RNA conformation. (**B**) Comparison of ^{19}F NMR spectra of *in vitro* sample of telomere RNA (up) with *Xenopus* egg lysates (middle) and in *Xenopus* oocytes (bottom).

samples (Figure 4B), indicating higher-order G-quadruplex formation in a cell-like condition.

Therefore, by using ^{19}F NMR spectroscopy, it was demonstrated that the telomere RNA G-quadruplexes preferentially adopt a stacked two-subunits G-quadruplex conformation rather than remaining as single-unit G-quadruplex in living cells. These findings provide the first insights into the structures of telomere RNA G-quadruplexes in the cellular environment.

^{19}F NMR analysis of telomere RNA G-quadruplexes in molecular crowding conditions

It is known that an intracellular environment was occupied with biological molecules of the cellular volume. A crowded environment (molecular crowding) has reported to influence the structural transition and thermodynamic stability of DNA G-quadruplexes (45,46). Recently, it is reported that ligands can specifically distinguish DNA multimeric G-quadruplexes from monomeric ones under molecular crowding conditions (47,48). To test whether the higher-order RNA G-quadruplex structure is promoted by the crowded environment, we used ^{19}F NMR spectroscopy to investigate the structural feature of telomere RNA G-quadruplex in K^+-containing crowded conditions, simulated by different cosolutes. We performed a concentration-dependent experiment to investigate the effect of molecular crowding conditions on the RNA G-quadruplex in crowded solution simulated by three organic solvents acetonitrile (ACN), dimethyl sulfoxide (DMSO) and ethanol (EtOH) at different concentrations (45,46). In the dilute solution (50 mM KCl water solution), one signal was observed at −62.91 ppm, indicating a dimeric parallel G-quadruplex formation, which is consistent with previously reported results (11–14). In crowded solutions of ACN, DMSO and EtOH, a new signal appeared when increasing the volume of cosolutes as compared with the dilute solution (Figure 5A–C). Furthermore, we employed a widely used cosolute PEG 200 to mimic steric crowing, showing the same result that one new signal appears (Figure 5D). This new signal was clearly observed, and its intensity increased remarkably at a cosolute volume of 40–50% (v/v) in four different types of crowded solutions. Each ^{19}F NMR signal arises as a result of the unique fluorine environment; thus, the presence of the two signals confirms the existence of two conformers

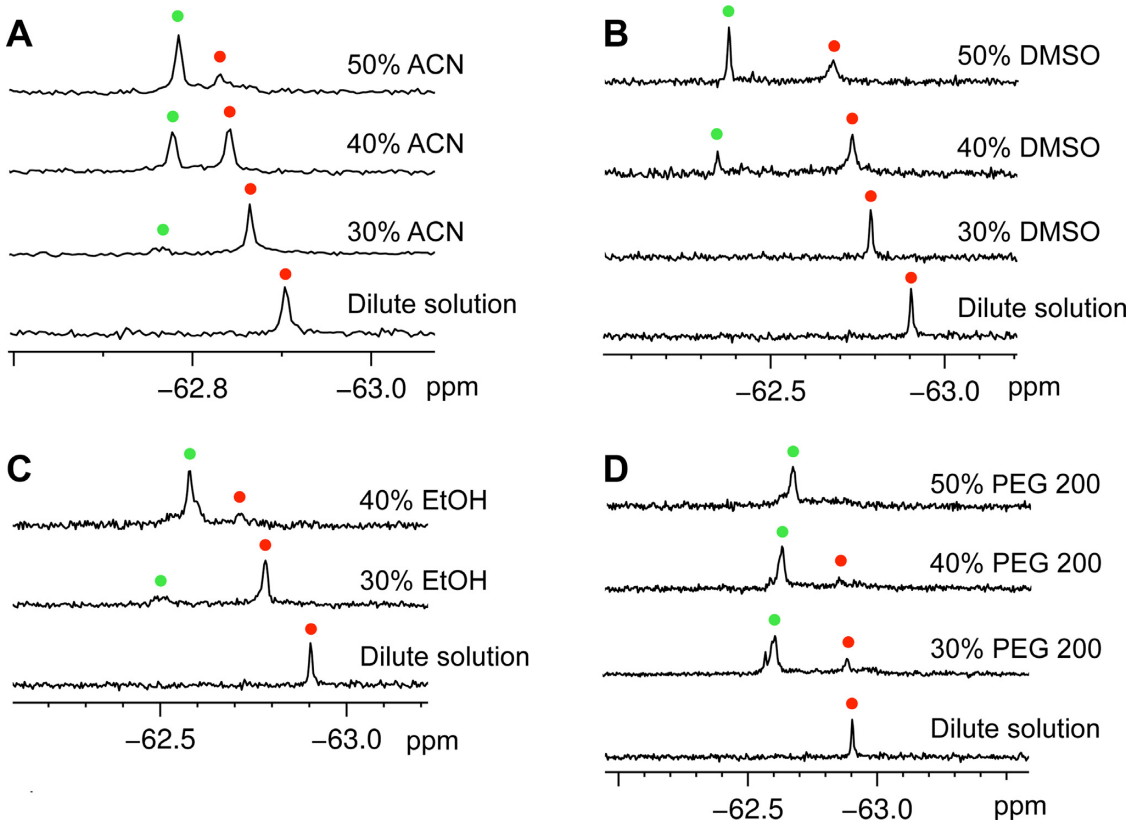

Figure 5. ^{19}F NMR of telomere RNA G-quadruplex in molecular crowding conditions. (**A**–**D**) ^{19}F NMR spectra of 12-mer telomere RNA (0.5 mM) in crowded solutions induced by (**A**) ACN, (**B**) DMSO, (**C**) EtOH and (**D**) PEG 200. ^{19}F NMR spectra were recorded under 30% (v/v), 40% (v/v) and 50% (v/v) of ACN, DMSO and PEG 200. The crowding condition of EtOH was only simulated by the addition of 30% (v/v) and 40% (v/v) EtOH, due to 50% (v/v) EtOH leading to a RNA precipitation. Red and green spots indicated the dimeric G-quadruplex and two-subunits stacked G-quadruplex. ^{19}F NMR reference spectrum of ^{19}F labeled 12-mer telomere RNA in dilute solution is shown in each case for comparison.

of the telomere RNA. Therefore, we assigned the new signal to the two-subunits stacked G-quadruplex structure based on the previous reports that molecular crowding could induce the formation of a multimer complex (44,49–54). It is notable that although the PEG 200 and organic solvents have different dielectric constant, polarity and other properties, all of these promote the formation of stacked dimeric G-quadruplex. Recently, several studies demonstrated the dehydration of organic solvents leads to the formation of parallel DNA G-quadruplex from other species (55–57). To combine our results and previous studies, we suggested that the exclusion effect and/or dehydration effect can promote the formation of high-order RNA G-quadruplex.

To further understand the effect of molecular crowding on RNA G-quadruplex structure, we measured the specific NMR signals by diluting high concentration RNA to 0.5 mM in diluted solution and molecular crowded condition. We found the transition of two-subunits stacked G-quadruplex to dimeric G-quadruplex is fast in diluted solution, while two-subunits stacked G-quadruplex is still stabilized at ∼0.5 mM under molecular crowded condition (Supplementary Figure S13), indicating that the observation of high-order G-quadruplex in living cells was due to the molecular crowding environment.

A temperature-dependent experiment was then performed to further confirm the assignment of the two signals that were observed in the ^{19}F NMR spectrum. Figure 6 shows that as the temperature increased from 23°C to 80°C in crowded solution of 40% and 50% (v/v) ACN, the peak intensity of the higher-order G-quadruplex decreased, whereas that of dimeric G-quadruplex increased, indicating the conversion of the higher-order to the dimeric G-quadruplex. In addition, upon heating to 55°C, a new peak corresponding to the unfolded single strand appeared and, at 80°C, only this peak remained with a strong intensity, whereas the peaks of the dimeric G-quadruplex and higher-order G-quadruplex nearly disappeared. These results indicate that at high temperatures, both G-quadruplexes unfolded to an unstructured single strand. Notably, the peak of the higher-order G-quadruplex in 50% (v/v) ACN had a higher intensity than that in 40% (v/v) ACN and still appeared at 75°C but not in 40% (v/v) ACN, indicating a higher thermal stability of the higher-order conformation in higher ratio of cosolutes. NMR data (Supplementary Figure S14) showed that a similar conformational transition could also occur in DMSO, PEG 200 and EtOH molecular crowding conditions under increased temperature. These observations suggest that molecular crowding induced the conformational transition from a dimeric G-quadruplex to a higher-order G-quadruplex structure. The results of T_m value show that molecular crowding substantially stabilizes the higher-order G-quadruplex structure in

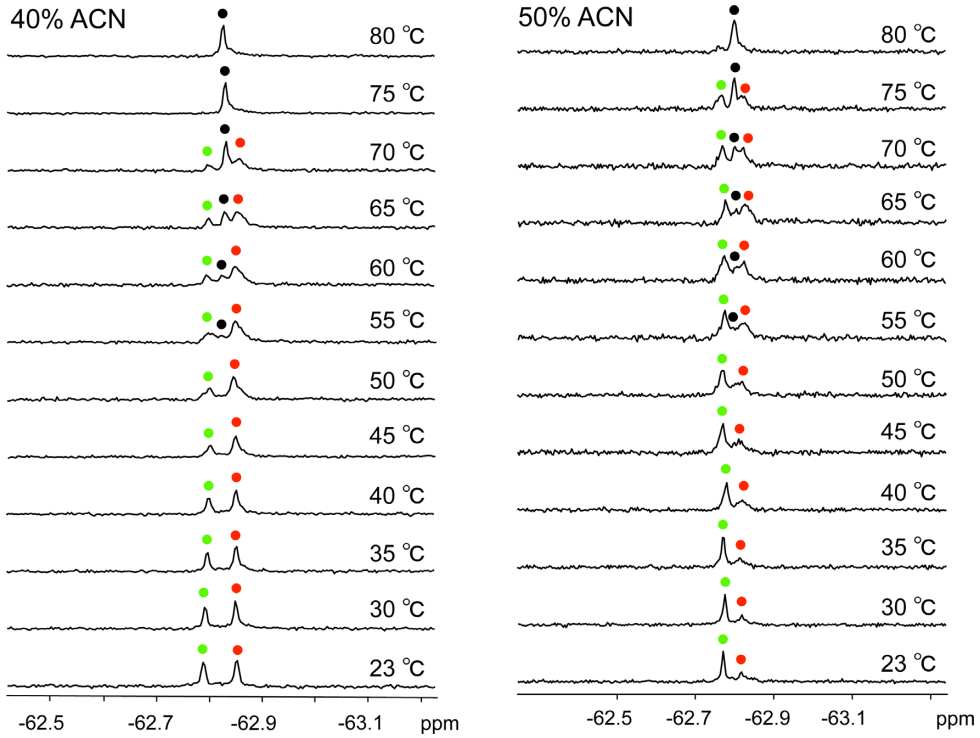

Figure 6. A temperature-dependent experiment of telomere RNA G-quadruplex in molecular crowding conditions. NMR spectra were recorded in crowded solution simulated by 40% (v/v) and 50% (v/v) of ACN. Condition: 0.5 mM RNA in 50 mM KCl and 10 mM Tris-HCl buffer (pH 7.0). The sample is kept for 10 min at each temperature. Red and green spots indicated the dimeric G-quadruplex and two-subunits stacked G-quadruplex. The peaks of single strand are marked with black spots. Temperatures indicated on the right.

Table 2. T_m for higher-order G-quadruplex in dilute and different crowded solutions

Conditions	T_m (°C)	ΔT_m (°C)
Dilute solution	52.4	–
40% ACN	58.6	6.2
50% ACN	69.5	17.1
40% DMSO	61.5	9.1
50% DMSO	76.2	23.8
40% PEG 200	56.8	4.4
50% PEG 200	61.9	9.5
40% EtOH	55.0	2.6

[a]The experimental errors for T_m were ±0.5°C.
3 mM RNA in diluted solution and 0.5 mM RNA in molecular crowding solution.

all types of crowded solutions, leading to an increase in T_m (ΔT_m = 2.6–23.8°C) as compared with the dilute solution (Figure 7 and Table 2). A greater stabilization of the higher-order G-quadruplex may result from the structural conversion of RNA G-quadruplex that is induced by the crowded solutions.

CONCLUSIONS

First, we showed that the simplicity and sensitivity of ^{19}F NMR spectroscopy effectively enables structural studies of telomere RNA G-quadruplexes *in vitro*. Using ^{19}F NMR spectroscopy, we directly observed the two-subunits stacked G-quadruplex, demonstrating that the two-subunits stacked G-quadruplex is formed predominantly at relatively high RNA concentration. Based on the sharp and clear ^{19}F NMR signals, we determined the thermodynamic parameters of the telomere RNA G-quadruplexes. We demonstrated that the stacking interactions of two G-quadruplex subunits provide the primary energetic contribution to the stability of higher-order RNA G-quadruplex at a level similar to that of a single G-tetrad. These results enable a better understanding of the formation of higher-order RNA G-quadruplexes.

Next, because there is no natural intracellular concentration of fluorine in cells, there is no background noise in in-cell ^{19}F NMR spectra. Therefore, ^{19}F NMR spectroscopy is an ideal tool for studying RNA G-quadruplex structures in living cells. We demonstrated that telomere RNA G-quadruplexes preferentially adopt a two-subunits stacked G-quadruplex in living cells using ^{19}F NMR spectroscopy. To our knowledge, this study is the first direct observation of higher-order RNA G-quadruplex in a cellular environment and provides new insight into the structural behavior of telomere RNA G-quadruplexes in living cells. Our results open new avenues for the investigation of G-quadruplex structures *in vitro* and in living cells.

Finally we demonstrated that molecular crowding conditions simulated by ACN, EtOH, DMSO and PEG 200 promoted the formation of two-subunits stacked G-quadruplex and stabilized the higher-order structure, which provided unequivocal evidence for the formation of higher-order G-quadruplex structure in living cells.

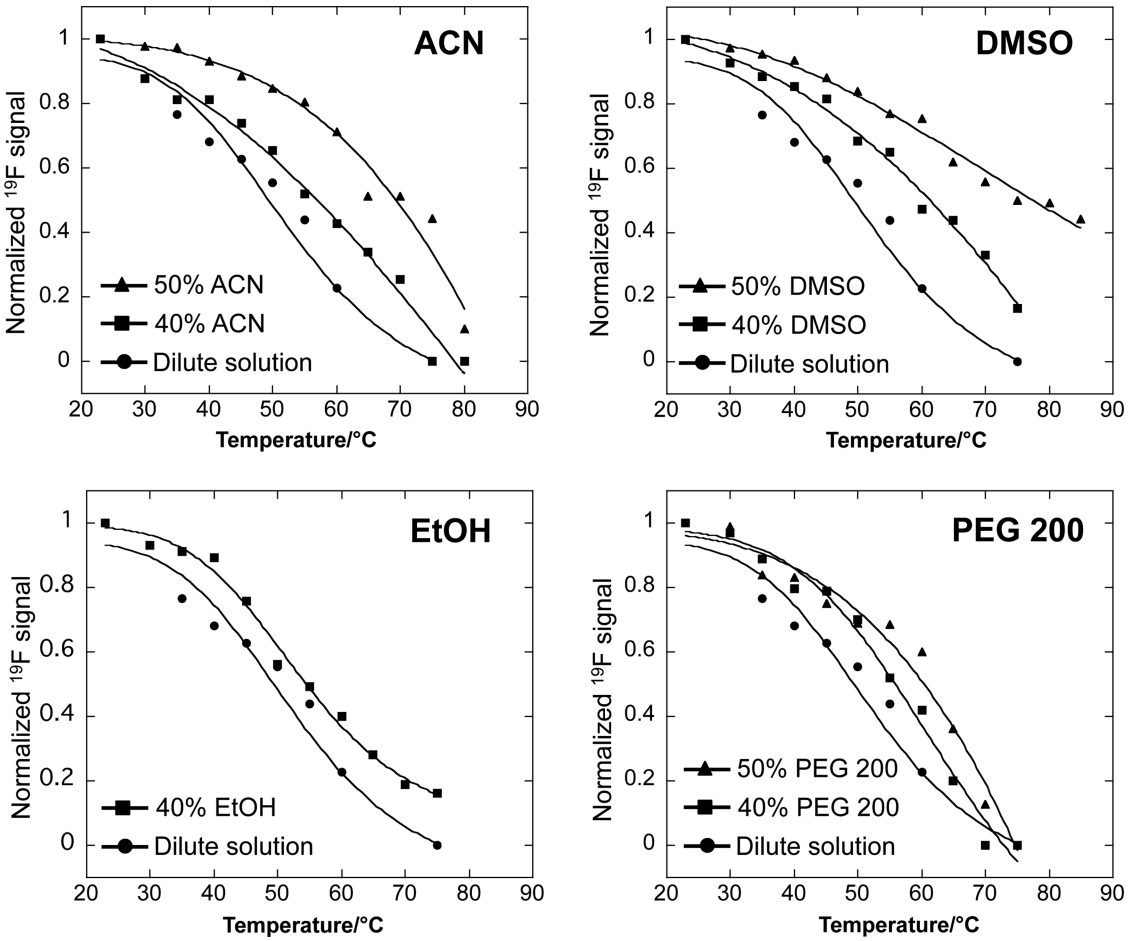

Figure 7. Melting profiles of the relative peak areas of the ^{19}F resonance signals versus temperature. The profiles were obtained by plotting the normalized two-subunits stacked G-quadruplex relative peak areas of the ^{19}F resonance signals in NMR spectra (Figure 2C, Figure 6 and Supplementary Figure S14) as a function of temperature.

SUPPLEMENTARY DATA

Supplementary Data are available at NAR Online.

ACKNOWLEDGEMENTS

This work was supported by a Grant-in-Aid for Scientific Research (B) (26288083) and a Grant-in-Aid for Research Activity Start-up (25888019) from the Ministry of Education, Science, Sports, Culture and Technology (Japan). This work was also supported by grants from the Takeda Science Foundation.

FUNDING

Grant-in-Aid for Scientific Research (B) and Research Activity Start-up from Ministry of Education, Science, Sports, Culture and Technology (Japan) [26288083 and 25888019]; Takeda Science Foundation. Funding for open access charge: Grant-in-Aid for Scientific Research (B) from the Ministry of Education, Science, Sports, Culture and Technology (Japan) [26288083].
Conflict of interest statement. None declared.

REFERENCES

1. Kertesz,M., Wan,Y., Mazor,E., Rinn,J.L., Nutter,R.C., Chang,H.Y. and Segal,E. (2010) Genome-wide measurement of RNA secondary structure in yeast. *Nature*, **467**, 103–107.
2. Wan,Y., Kertesz,M., Spitale,R.C., Segal,E. and Chang,H.Y. (2011) Understanding the transcriptome through RNA structure. *Nat. Rev. Genet.*, **12**, 641–655.
3. Ding,Y., Tang,Y., Kwok,C.K., Zhang,Y., Bevilacqua,P.C. and Assmann,S.M. (2014) *In vivo* genome-wide profiling of RNA secondary structure reveals novel regulatory features. *Nature*, **505**, 696–700.
4. Collie,G.W. and Parkinson,G.N. (2011) The application of DNA and RNA G-quadruplexes to therapeutic medicines. *Chem. Soc. Rev.*, **40**, 5867–5892.
5. Xu,Y. (2011) Chemistry in human telomere biology: structure, function and targeting of telomere DNA/RNA. *Chem. Soc. Rev.*, **40**, 2719–2740.
6. Balk,B., Maicher,A., Dees,M., Klermund,J., Luke-Glaser,S., Bender,K. and Luke,B. (2013) Telomeric RNA-DNA hybrids affect telomere-length dynamics and senescence. *Nat. Struct. Mol. Biol.*, **20**, 1199–1205.
7. Haeusler,A.R., Donnelly,C.J., Periz,G., Simko,E.A., Shaw,P.G., Kim,M.S., Maragakis,N.J., Troncoso,J.C., Pandey,A., Sattler,R. *et al.* (2014) *C9orf72* nucleotide repeat structures initiate molecular cascades of disease. *Nature*, **507**, 195–200.
8. Wolfe,A.L., Singh,K., Zhong,Y., Drewe,P., Rajasekhar,V.K., Sanghvi,V.R., Mavrakis,K.J., Jiang,M., Roderick,J.E., Van der

Meulen,J. *et al.* (2014) RNA G-quadruplexes cause eIF4A-dependent oncogene translation in cancer. *Nature*, **513**, 65–70.
9. Azzalin,C.M., Reichenbach,P., Khoriauli,L., Giulotto,E. and Lingner,J. (2007) Telomeric repeat-containing RNA and RNA surveillance factors at mammalian chromosome ends. *Science*, **318**, 798–801.
10. Schoeftner,S. and Blasco,M.A. (2008) Developmentally regulated transcription of mammalian telomeres by DNA-dependent RNA polymerase II. *Nat. Cell Biol.*, **10**, 228–236.
11. Xu,Y., Kaminaga,K. and Komiyama,M. (2008) G-quadruplex formation by human telomeric repeats-containing RNA in Na^+ solution. *J. Am. Chem. Soc.*, **130**, 11179–11184.
12. Martadinata,H. and Phan,A.T. (2009) Structure of propeller-type parallel-stranded RNA G-quadruplexes, formed by human telomeric RNA sequences in K^+ solution. *J. Am. Chem. Soc.*, **131**, 2570–2578.
13. Xu,Y., Ishizuka,T., Kimura,T. and Komiyama,M. (2010) A U-tetrad stabilizes human telomeric RNA G-quadruplexstructure. *J. Am. Chem. Soc.*, **132**, 7231–7233.
14. Xu,Y., Suzuki,Y., Ito,K. and Komiyama,M. (2010) Telomeric repeat-containing RNA structure in living cells. *Proc. Natl. Acad. Sci. U.S.A.*, **107**, 14579–14584.
15. Xu,Y., Ishizuka,T., Yang,J., Ito,K., Katada,H., Komiyama,M. and Hayashi,T. (2012) Oligonucleotide models of telomeric DNA and RNA form a Hybrid G-quadruplex structure as a potential component of telomeres. *J. Biol. Chem.*, **287**, 41787–41796.
16. Collie,G.W., Parkinson,G.N., Neidle,S., Rosu,F., De Pauw,E. and Gabelica,V. (2010) Electrospray mass spectrometry of telomeric RNA (TERRA) reveals the formation of stable multimeric G-quadruplex structures. *J. Am. Chem. Soc.*, **132**, 9328–9334.
17. Martadinata,H. and Phan,A.T. (2013) Structure of human telomeric RNA (TERRA): stacking of two G-quadruplex blocks in K^+ solution. *Biochemistry*, **52**, 2176–2183.
18. Zhou,L., Rajabzadeh,M., Traficante,D.D. and Cho,B.P. (1997) Conformational heterogeneity of arylamine-modified DNA: ^{19}F NMR evidence. *J. Am. Chem. Soc.*, **119**, 5384–5389.
19. Hammann,C., Norman,D.G. and Lilley,D.M. (2001) Dissection of the ion-induced folding of the hammerhead ribozyme using ^{19}F NMR. *Proc. Natl. Acad. Sci. U.S.A.*, **98**, 5503–5508.
20. Scott,L.G., Geierstanger,B.H., Williamson,J.R. and Hennig,M. (2004) Enzymatic synthesis and ^{19}F NMR studies of 2-fluoroadenine-substituted RNA. *J. Am. Chem. Soc.*, **126**, 11776–11777.
21. Olsen,G.L., Edwards,T.E., Deka,P., Varani,G., Sigurdsson,S.T. and Drobny,G.P. (2005) Monitoring tat peptide binding to TAR RNA by solid-state ^{31}P-^{19}F REDOR NMR. *Nucleic Acids Res.*, **33**, 3447–3454.
22. Hennig,M., Scott,L.G., Sperling,E., Bermel,W. and Williamson,J.R. (2007) Synthesis of 5-fluoropyrimidine nucleotides as sensitive NMR probes of RNA structure. *J. Am. Chem. Soc.*, **129**, 14911–14921.
23. Barhate,N.B., Barhate,R.N., Cekan,P., Drobny,G. and Sigurdsson,S.T. (2008) A nonafluoro nucleoside as a sensitive ^{19}F NMR probe of nucleic acid conformation. *Org. Lett.*, **10**, 2745–2747.
24. Graber,D., Moroder,H. and Micura,R. (2008) ^{19}F NMR spectroscopy for the analysis of RNA secondary structure populations. *J. Am. Chem. Soc.*, **130**, 17230–17231.
25. Kiviniemi,A. and Virta,P. (2010) Characterization of RNA invasion by ^{19}F NMR spectroscopy. *J. Am. Chem. Soc.*, **132**, 8560–8562.
26. Sakamoto,T., Hayakawa,H. and Fujimoto,K. (2011) Development of a potassium ion sensor for ^{19}F magnetic resonance chemical shift imaging based on fluorine-labeled thrombin aptamer. *Chem. Lett.*, **40**, 720–721.
27. Fauster,K., Kreutz,C. and Micura,R. (2012) 2′-SCF_3 uridine-a powerful label for probing structure and function of RNA by ^{19}F NMR spectroscopy. *Angew. Chem. Int. Ed.*, **51**, 13080–13084.
28. Lombes,T., Moumne,R., Larue,V., Prost,E., Catala,M., Lecourt,T., Dardel,F., Micouin,L. and Tisne,C. (2012) Investigation of RNA-ligand interactions by ^{19}F NMR spectroscopy using fluorinated probes. *Angew. Chem. Int. Ed.*, **51**, 9530–9534.
29. Chen,H., Viel,S., Ziarelli,F. and Peng,L. (2013) ^{19}F NMR: a valuable tool for studying biological events. *Chem. Soc. Rev.*, **42**, 7971–7982.
30. Tanabe,K., Tsuda,T., Ito,T. and Nishimoto,S. (2013) Probing DNA mismatched and bulged structures by using ^{19}F NMR spectroscopy and oligodeoxynucleotides with an ^{19}F-labeled nucleobase. *Chem. Eur. J.*, **19**, 15133–15140.
31. Granqvist,L. and Virta,P. (2014) 4′-*C*-[(4-trifluoromethyl-1*H*-1,2,3-triazol-1-yl)methyl]thymidine as a sensitive ^{19}F NMR sensor for the detection of oligonucleotide secondary structures. *J. Org. Chem.*, **79**, 3529–3536.
32. Zhao,C., Devany,M. and Greenbaum,N.L. (2014) Measurement of chemical exchange between RNA conformers by ^{19}F NMR. *Biochem. Biophys. Res. Commun.*, **453**, 692–695.
33. Zimmerman,S.B. and Trach,S.O. (1991) Estimation of macromolecule concentrations and excluded volume effects for the cytoplasm of Escherichia coli. *J. Mol. Biol.*, **222**, 599–620.
34. Ellis,R.J. and Minton,A.P. (2003) Cell biology: join the crowd. *Nature*, **425**, 27–28.
35. Zhou,H.X., Rivas,G. and Minton,A.P. (2008) Macromolecular crowding and confinement: biochemical, biophysical, and potential physiological consequences. *Annu. Rev. Biophys.*, **37**, 375–397.
36. Sakai,T., Tochio,H., Tenno,T., Ito,Y., Kokubo,T., Hiroaki,H. and Shirakawa,M. (2006) In-cell NMR spectroscopy of proteins inside *Xenopus laevis* oocytes. *J. Biomol. NMR*, **36**, 179–188.
37. Serber,Z., Selenko,P., Hansel,R., Reckel,S., Lohr,F., Ferrell,J.E. Jr, Wagner,G. and Dotsch,V. (2006) Investigating macromolecules inside cultured and injected cells by in-cell NMR spectroscopy. *Nat. Protoc.*, **1**, 2701–2709.
38. Selenko,P., Serber,Z., Gadea,B., Ruderman,J. and Wagner,G. (2006) Quantitative NMR analysis of the protein G B1 domain in *Xenopus laevis* egg extracts and intact oocytes. *Proc. Natl. Acad. Sci. U.S.A.*, **103**, 11904–11909.
39. Sakakibara,D., Sasaki,A., Ikeya,T., Hamatsu,J., Hanashima,T., Mishima,M., Yoshimasu,M., Hayashi,N., Mikawa,T., Walchli,M. *et al.* (2009) Protein structure determination in living cells by in-cell NMR spectroscopy. *Nature*, **458**, 102–105.
40. Hansel,R., Foldynova-Trantirkova,S., Lohr,F., Buck,J., Bongartz,E., Bamberg,E., Schwalbe,H., Dotsch,V. and Trantirek,L. (2009) Evaluation of parameters critical for observing nucleic acids inside living *Xenopus laevis* oocytes by in-cell NMR spectroscopy. *J. Am. Chem. Soc.*, **131**, 15761–15768.
41. Allen,T.D., Rutherford,S.A., Murray,S., Sanderson,H.S., Gardiner,F., Kiseleva,E., Goldberg,M.W. and Drummond,S.P. (2007) A protocol for isolating Xenopus oocyte nuclear envelope for visualization and characterization by scanning electron microscopy (SEM) or transmission electron microscopy (TEM). *Nat. Protoc.*, **2**, 1166–1172.
42. Halley-Stott,R.P., Pasque,V., Astrand,C., Miyamoto,K., Simeoni,I., Jullien,J. and Gurdon,J.B. (2010) Mammalian nuclear transplantation to Germinal Vesicle stage Xenopus oocytes-a method for quantitative transcriptional reprogramming. *Methods*, **51**, 56–65.
43. Selenko,P. and Wagner,G. (2007) Looking into live cells with in-cell NMR spectroscopy. *J. Struct. Biol.*, **158**, 244–253.
44. Hansel,R., Lohr,F., Foldynova-Trantirkova,S., Bamberg,E., Trantirek,L. and Dotsch,V. (2011) The parallel G-quadruplex structure of vertebrate telomeric repeat sequences is not the preferred folding topology under physiological conditions. *Nucleic Acids Res.*, **39**, 5768–5775.
45. Yu,H., Gu,X., Nakano,D., Miyoshi,D. and Sugimoto,N. (2012) Beads-on-a-string structure of long telomeric DNAs under molecular crowding conditions. *J. Am. Chem. Soc.*, **134**, 20060–20069.
46. Heddi,B. and Phan,A.T. (2011) Structure of human telomeric DNA in crowded solution. *J. Am. Chem. Soc.*, **133**, 9824–9833.
47. Huang,X.X., Zhu,L.N., Wu,B., Huo,Y.F., Duan,N.N. and Kong,D.M. (2014) Two cationic porphyrin isomers showing different multimeric G-quadruplex recognition specificity against monomeric G-quadruplexes. *Nucleic Acids Res.*, **42**, 8719–8731.
48. Zhang,Q., Liu,Y.C., Kong,D.M. and Guo,D.S. (2015) Tetraphenylethene derivatives with different numbers of positively charged side arms have different multimeric G-quadruplex recognition specificity. *Chem. Eur. J.*, **21**, 13253–13260.
49. Minton,A.P. (1981) Excluded volume as a determinant of macromolecular structure and reactivity. *Biopolymers*, **20**, 2093–2120.
50. Zimmerman,S.B. and Minton,A.P. (1993) Macromolecular crowding: biochemical, biophysical, and physiological consequences *Annu. Rev. Biophys. Biomol. Struct.*, **22**, 27–65.
51. Wenner,J.R. and Bloomfield,V.A. (1999) Crowding effects on EcoRV kinetics and binding. *Biophys. J.*, **77**, 3234–3241.
52. Davis-Searles,P.R., Saunders,A.J., Erie,D.A., Winzor,D.J. and Pielak,G.J. (2001) Interpreting the effects of small uncharged solutes

on protein-folding equilibria. *Annu. Rev. Biophys. Biomol. Struct.*, **30**, 271–306.
53. Minton,A.P. (2011)The influence of macromolecular crowding and macromolecular confinement on biochemical reactions in physiological media. *J. Biol. Chem.*, **276**, 10577–10580.
54. Miyoshi,D., Karimata,H. and Sugimoto,N. (2005) Drastic effect of a single base difference between human and tetrahymena telomere sequences on their structures under molecular crowding conditions. *Angew. Chem. Int. Ed.*, **44**, 3740–3744.
55. Buscaglia,R., Miller,M.C., Dean,W.L., Gray,R.D., Lane,A.N., Trent,J.O. and Chaires,J.B. (2013) Polyethylene glycol binding alters human telomere G-quadruplex structure by conformational selection. *Nucleic Acids Res.*, **41**, 7934–7946.
56. Dhakal,S., Cui,Y., Koirala,D., Ghimire,C., Kushwaha,S., Yu,Z., Yangyuoru,P.M. and Mao,H. (2013) Structural and mechanical properties of individual human telomeric G-quadruplexes in molecularly crowded solutions. *Nucleic Acids Res.*, **41**, 3915–3923.
57. Miller,M.C., Buscaglia,R., Chaires,J.B., Lane,A.N. and Trent,J.O. (2010) Hydration is a major determinant of the G-Quadruplex stability and conformation of the human telomere 3′ sequenc of d(AG_3($TTAG3)_3$). *J. Am. Chem. Soc.*, **132**, 17105–17107.